Performance improvement of shunt active power filter based on non-linear least-square approach

Terriche, Yacine; Guerrero, Josep M.; Quintero, Juan Carlos Vasquez

Published in:
Electric Power Systems Research

DOI (link to publication from Publisher):
10.1016/j.epsr.2018.02.004

Publication date:
2018

Document Version
Accepted author manuscript, peer reviewed version

A Non-Linear Least-Square-Based Reference Compensating Current Generation for Three-Phase Shunt Active Power Filter

Yacine Terriche, Josep M. Guerrero, Juan C. Vasquez
Department of Energy Technology, Aalborg University, Aalborg, Denmark
(yte@et.aau.dk; joz@et.aau.dk; juq@et.aau.dk)

***Abstract*—Nowadays, the shunt Active power filters (SAPFs) have become a popular solution for power quality issues. A crucial issue in controlling the SAPFs which is highly correlated with their accuracy, flexibility and dynamic behavior, is generating the reference compensating current (RCC). The synchronous reference frame (SRF) approach is widely used for generating the RCC due to its simplicity and computation efficiency. However, the SRF approach needs precise information of the voltage phase which becomes a challenge under adverse grid conditions. A typical solution to answer this need is the application of advanced phase locked loops (PLLs). The PLLs are closed-loop control systems that often have a response time more than two cycles of the nominal frequency. Besides, a special care should be paid in designing their control parameters to ensure their stable operation in all circumstances. This paper proposes an improved open loop strategy which is unconditionally stable and flexible. The proposed method which is based on non-linear least square (NLS) approach, can extract the fundamental voltage and estimates its phase within only half cycle, even in the presence of odd harmonics and dc offset. The performance of the proposed method is verified experimentally and compared with advanced PLLs.**

***Index Terms*— Moving average filters (MAFs), multiple complex-coefficient filters (MCCFs), non-linear least square (NLS) approach, phase locked loop, power quality issues, synchronization, shunt active power filter (SAPF).**

I. Introduction

THE augmented application of electronic devices applied to the power conversion cause hazardous consequences to the power quality (PQ) of both transmission and distribution levels. The non-linear characteristics of these devices that are based on semi-conductors can cause harmonic contamination by drawing a non-sinusoidal current from the power supply [1]. Traditionally, passive power filters (PPF) are installed to mitigate the most dominant harmonics, and compensate for the reactive content needed by the loads. Although, this solution is characterized by the simplicity, low cost and easy maintenance, it cannot be a reliable solution because it highly depends on the grid impedance, which has a varying nature. Besides, PPFs are highly sensitive to variations in the load parameters and are prone to resonance with the line/load impedance. [2]. To overcome these drawbacks, the shunt active power filters (SAPFs) have received much attention to be an alternative solution for PQ issues [3]. The SAPF is able to compensate for the harmonic contents, reactive power and unbalance, with a fast dynamic behavior and flexibility during the load variations.

The algorithm of identifying the reference compensating current (RCC) is a key factor for the dynamic behavior and preciseness of the SAPFs. In the frequency domain, probably the discrete Fourier transform (DFT) and the fast Fourier transform (FFT) are broadly used [4], [5]. The DFT is a mathematical transform of a discrete signal with the number of points N, while the FFT is a faster version of the DFT with an efficient algorithm to perform the DFT with a faster computation. The FFT however requires additional power because of computing all the frequency bins during the process [6]. Furthermore, the difficulty in calculating the inter-harmonics, the picket-fence effect and spectral leakage are weakness for this technique. In the time domain, the instantaneous reactive power (P-Q) theory and the synchronous reference frame (SRF) methods are widely used [7], [8]. Both methods are well-known by their simplicity and efficacy under steady state and transient operations. Moreover, the power factor (PF) and current unbalance are easily compensated using time domain methods. The SRF approach is considered more advantageous technique than the P-Q theory in terms of harmonic selectivity. The basic principle of the SRF approach is to use the phase locked loop (PLL) to synchronize the RCC with the voltage. Extracting the fundamental is achieved by estimating the angular frequency of the fundamental component of the voltage using the PLL to perform Park transform. Consequently, the fundamental component of the distorted current appears as a dc component in the *dq* coordinate, while the rest harmonics appear as ripples. The RCC is obtained by separating the ripples from the dc component and transforming it back to the *abc* frame. The separation can be achieved using a low-pass filter, moving average filter, or other techniques.

The SRF method however, offers poor performance under adverse grid conditions. Several pre-filtering and synchronization techniques can be applied to the voltage are proposed in the literature [9], such as: Kalman filter based synchronization method [10], the zero crossing detecting methods [11], frequency locked loop based technique [12], geometric template matching and recurrent artificial neural network [13] and least mean square based method [14]. Other techniques apply advanced PLLs such as

[15]: moving average filters (MAF) based PLL [16]-[19], delayed signal cancellation (DSC) operator based-PLL [20], decoupled double synchronous reference frame (DDSRF) based PLL [21], second-order generalized integrator (SOGI) [22], variable sampling period filter (VSPF) based PLL [23], multiple-complex coefficient-filter-based PLL (MCCF) [24]. However, most of these techniques depend on digital or complex filters that make a tradeoff between the dynamic response and the preciseness. As a consequence, obtaining an accurate estimation of the voltage phase, results in a large transient response that can exceed two cycles under adverse grid conditions. Moreover, the synchronization techniques based on PLL are a closed loop control system that requires a special care in designing its controller gains to avoid instability under all circumstances.

This paper proposes a novel synchronization strategy based on NLS approach applied as a pre-filtering stage to estimate the voltage phase. The methodology is based on transforming the voltage to $\alpha\beta$ stationary reference frame using Clark transform. The main advantage of this transform is to reduce the number of filters which results in decreasing the computation burden. Then, the transformed voltage passes through a derivative to cancel any appearance of the dc offset. Using a derivative with digital and complex filters to cancel the dc offset affects their accuracy due to the amplification of noise. However, it will be demonstrated in this paper that the NLS approach provides an accurate estimation of the fundamental component and its phase, even under noise contaminated signal. Consequently, the voltage phase can be estimated within a half cycle even in the presence of harmonic components, unbalance and dc offset, which results in optimizing the dynamic response, the accuracy and the flexibility of the SAPF with less computation burden. The effectiveness of the proposed technique is verified by experimental results, and compared with advanced PLLs (MCCF-PLL and MAF-PLL) under unbalanced and distorted voltage.

This paper is organized as follows: Section II introduces overviews of the MAF-PLL, MCCF-PLL and NLS approach. Section III describes the proposed method. In Section IV, the practical results are presented and discussed. And Section V concludes this paper.

II. SYNCHRONIZATION AND PHASE ESTIMATION USING MAF-PLL, MCCF-PLL AND NLS APPROACH

1. MAF-PLL overview

Probably, one of the most used synchronization techniques in three-phase systems is the synchronous rotating frame PLL (SRF-PLL) [15]. It benefits from several advantages such as: simplicity, fast response, accurate phase detection and efficient performance under ideal grid conditions [9]. However, under adverse grid conditions, it introduces poor phase/frequency estimation [16]. This problem can be mitigated by decreasing the size of the loop bandwidth, but this solution will be on the cost of the dynamic response and rapidity of tracking the phase and frequency. Moreover, it may not be a good solution to reject the grid voltage imbalance [16], [9].

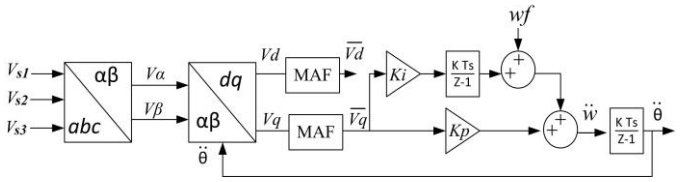

Fig. 1. Basic scheme of MAF-PLL

Several solutions have been recently proposed to overcome the weaknesses of the SRF-PLL under adverse grid conditions. These solutions are based on using some filtering stages such as pre-filtering techniques to the input signal, or in-loop techniques inside the phase loop [9], [25]. Incorporating the moving average filter (MAF) within the phase control loop of the PLL is relatively recent [17], [19]. Fig. 1 shows the block diagram of the MAF-PLL where $v_{s1,2,3}$ is the three-phase voltage, w_f is the fundamental frequency and it is set to 2π50 rad/s, $\hat{w}$ is the estimated grid frequency and $\hat{\theta}$ is the estimated phase.

Equations (1)-(6) show the modeled grid voltage that is assumed to be unbalanced and harmonically contaminated, introducing v^p (v^n) and $\acute{\emptyset}^p$($\acute{\emptyset}^n$) as the amplitude and the phase angle of the positive-(negative) sequence of the fundamental, $\tilde{v}^p$ ($\tilde{v}^n$) and $\tilde{\theta}^p$ ($\tilde{\theta}^n$) are the amplitude and the phase angle of the positive-(negative) sequence of the harmonics, v_{dof} is the dc offset component, p and n refer respectively to the positive and negative sequences, h is the harmonic order, m =1,2,3 and k =0,-1,1.

$$v_{sm} = \left[v_{dof} + v_{mf}^{p} + v_{mf}^{n} + \sum [v_{mh}^{p} + v_{mh}^{n}]\right] \tag{1}$$

$$\left[v_{mf}^{p} + v_{mf}^{n}\right] =$$

$$\left[v_{m}^{p}\, cos\left(\acute{\emptyset}_{m}^{p} + k\frac{2\pi}{3}\right) + v_{m}^{n}\, cos\left(\acute{\emptyset}_{m}^{n} + k\frac{2\pi}{3}\right)\right] \tag{2}$$

$$\sum \left[v_{mh}^{p} + v_{mh}^{n}\right] =$$

$$\left[\tilde{v}_{mh}^{p}\, cos\left(\tilde{\theta}_{mh}^{p} + k\frac{2\pi}{3}\right) + \tilde{v}_{mh}^{n}\, cos\left(\tilde{\theta}_{mh}^{n} + k\frac{2\pi}{3}\right)\right] \tag{3}$$

The grid voltage can be expressed on *αβ* stationary reference frame by applying Clarke transform as

$$\begin{bmatrix} v_\alpha \\ v_\beta \end{bmatrix} = \begin{bmatrix} v_\alpha^p \\ v_\beta^p \end{bmatrix} + \begin{bmatrix} v_\alpha^n \\ v_n^p \end{bmatrix} = \frac{2}{3}\begin{bmatrix} 1 & \frac{-1}{2} & \frac{-1}{2} \\ 0 & \frac{\sqrt{3}}{2} & \frac{-\sqrt{3}}{2} \end{bmatrix} \begin{bmatrix} v_{s1} \\ v_{s2} \\ v_{s3} \end{bmatrix} \tag{4}$$

Then Park transform can be applied as shown bellow

$$\begin{bmatrix} v_d \\ v_q \end{bmatrix} = \begin{bmatrix} v_d^p \\ v_q^p \end{bmatrix} + \begin{bmatrix} v_d^n \\ v_q^p \end{bmatrix} = \begin{bmatrix} cos(\hat{\theta}^p) & sin(\hat{\theta}^p) \\ -sin(\hat{\theta}^p) & cos(\hat{\theta}^p) \end{bmatrix} \begin{bmatrix} v_\alpha \\ v_\beta \end{bmatrix} \tag{5}$$

where $\hat{\theta} = \hat{w}t$.

Under a quasi-locked condition ($\hat{\theta}^p \approx \acute{\emptyset}^p, \hat{w} = w$) equation (5) becomes

$$\begin{bmatrix} v_d \\ v_q \end{bmatrix} = \begin{bmatrix} v_{ddc} \\ v_{qdc} \end{bmatrix} + \begin{bmatrix} v_{dac} \\ v_{qac} \end{bmatrix} \tag{6}$$

where v_{ddc} and v_{qdc} are the dc terms that respectively provide information of v_s^p and the phase error, while v_{dac} and v_{qac} are the ripples. Extracting v_{ddc} and v_{qdc} from v_{dac} and v_{qac} can be attained by passing through the MAF as depicted in Fig. 1.

The expression of the MAF can be expressed in continues domain and discrete domain as shown respectively

$$B(t) = \frac{1}{T_w} \int_{t-T_w}^{t} A(\tau)\ d\tau \tag{7}$$

$$B(k) = \frac{1}{N} \sum_{n=0}^{N-1} A(k-n) \tag{8}$$

where A and B are respectively the input and the output signals, T_w is the window width, N is the number of points that is corresponding to the window width. In Laplace domain, the MAF is expressed as:

$$MAF_G = \frac{B(s)}{A(s)} = \frac{1 - e^{-T_w s}}{T_w s} \tag{9}$$

According to Padé approximation the delay time of (9) can be approximated as shown below

$$e^{-T_w s} \approx \frac{1 - \frac{-T_w s}{2}}{T_w s + \frac{-T_w s}{2}} \tag{10}$$

Then substituting (10) in (9) results in

$$MAF_G \approx \frac{1}{1 + \frac{T_w s}{2}} \tag{11}$$

In most application, the grid frequency varies within a small limit, if we neglect the error caused by this variation, then the input signal will contain frequency components that are integer multiple of the fundamental ($f = \frac{1}{T_w}$), therefore the MAF can be considered as an ideal low-pass filter if T_w is appropriately selected.

Substituting $s = jw = j2\pi f$, the magnitude and phase margin of the MAF can be expressed as

$$|G_{MAF}(j2\pi f)| = \left| \frac{\sin(\pi f T_w)}{\pi f T_w} \right| \tag{12}$$

$$\emptyset|G_{MAF}(j2\pi f)| = -\pi f T_w \tag{13}$$

$$|G_{MAF}(e^{j2\pi f T_s})| = \left| \frac{\sin(\pi f N T_s)}{N sin(\pi f T_w)} \right| \tag{14}$$

$$|G_{MAF}(j2\pi f)| = -\pi f T_s(N-1) \quad (15)$$

The width of T_w defines the mean value of the assembled data that extracts the dc signal which is corresponding to the fundamental component. The selection of T_w is achieved accordingly to the order of existing harmonics, the larger T_w is, the longer dynamic response. Fig. 2. shows the Bode diagram of the MAF with three different sizes of T_w (0.02/6 s, 0.01s and 0.02s), it is clear that the MAF can only be tuned to eliminate the harmonics of the order 6h$\pm$1 when T_w =0.02/6s, and it can add extra frequencies tuning for the odd harmonics caused by the unbalance when T_w =0.01s, whereas setting T_w =0.02s extends the tuning of the MAF to eliminate the even harmonics and the dc offset.

Fig. 3. shows the transient response of the MAF Fig. 3. (a) depicts the case where the grid voltage contains the harmonic components of the order 6h$\pm$1, in Fig. 3 (b) the unbalance is added and in Fig. 3 (c) the grid voltage is contaminated with the harmonic components and the dc offset. It is obvious in the first case (Fig. 3 (a)) when T_w is set to 0.02/6s, the MAF provides the faster transient response with the same accuracy of the other selections. While in the existing of the unbalance (Fig. 3. (b)) setting T_w to 0.01s offers the faster response that gives satisfactory accuracy. However, In the appearance of the dc offset (Fig. 3. (b)), setting T_w to $0.02s$ is mandatory to obtain a sufficient accuracy.

The disadvantage of the SRF-PLL lies in the transient response of V_q that depends on the instant v_β is measured. Fig. 4 shows v_β that is considered sinusoidal and started with three different phases ($0^o, 120^o$ and 180^o), it is obvious that when v_β starts from 0^o, V_q has neglected transient response. However, when v_β starts from 120^o and 180^o, V_q takes respectively more than one and two cycles to reach steady state. In case v_β contain harmonics, implementing the MAF require longer transient response to offer accurate information.

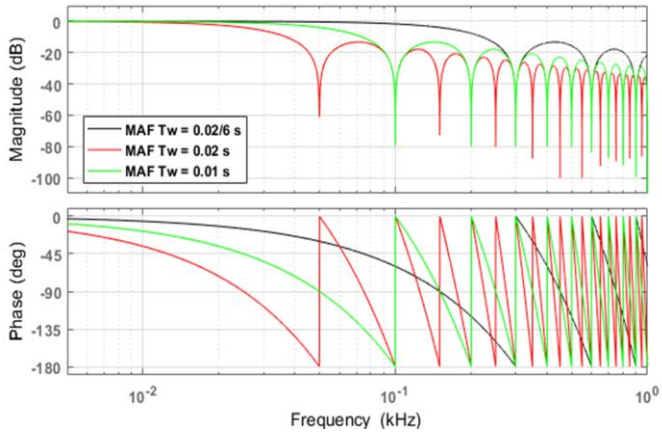

Fig. 2. Bode plot of MAF at $T_w = 0.02s, 0.0s1$ and 0.02/6s

The designing of the PI controller is established using the open-loop transfer function of the MAF-PLL that is shown bellow

$$G_p = v^p \frac{1}{1+\frac{T_w s}{2}} \frac{(k_p s + k_i)}{s} \frac{1}{s} \tag{16}$$

$$G_p \approx v^p \frac{\frac{2}{T_w}(k_p s + k_i)}{s^2\left(s+\frac{2}{T_w}\right)} \tag{17}$$

According to [16], the PLL can reach optimum performance when

$$\frac{2}{T_w} = bw_c \tag{18}$$

$$k_p = \frac{w_c}{v^p} \tag{19}$$

$$k_i = \frac{{w_c}^2}{bv^p} \tag{20}$$

where w_c is the crossover frequency, b is a constant selected to adjust both phase margin and transient response speed. In [16]

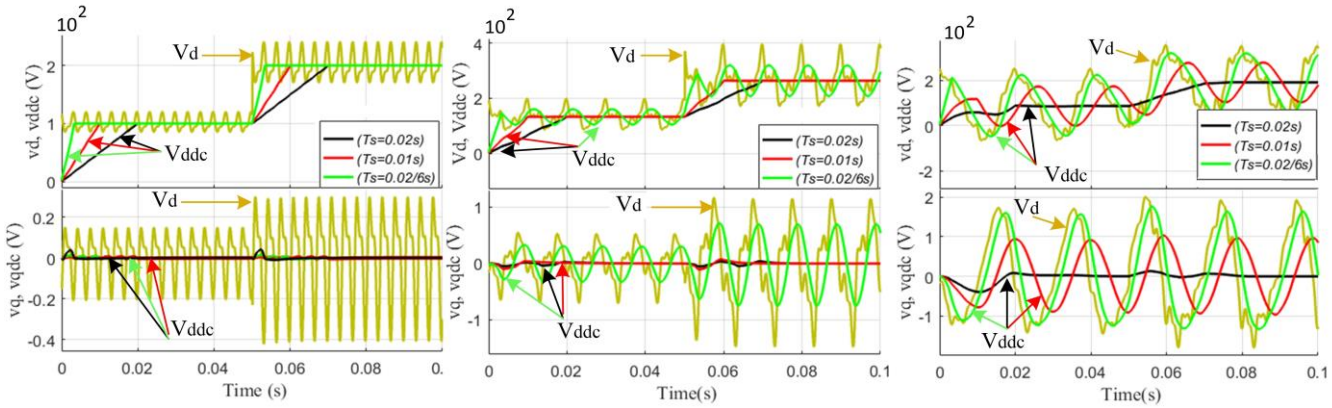

(a) (b) (c)

Fig. 3. Performance example of MAF at $T_w = 0.02s, 0.01$ and $0.02/6s$. (a) Existence of harmonics of the order $6h \pm 1$ in the grid voltage. (b) Unbalanced and contaminated grid voltage. (c) Existence of harmonics and dc offset.

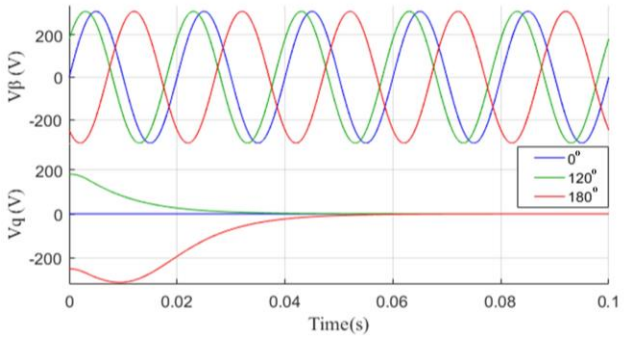

Fig. 4. Transient response of V_q in case of three different phases of v_β

and [18], the value of b is set to $1 + 1/\sqrt{2}$ to satisfy both transient response speed and sufficient stability margin.

2. MCCF-PLL overview

The MCCF-PLL is distinguished from other advanced SRF-PLLs by the integration of complex-coefficient filters (CCFs) [24]. In contradiction with the real coefficient filters (RCFs) such as band-pass filters (BPFs) that only have frequency selectivity characteristic, the CFFs provide both properties frequency and sequence-selective [24], [25]. In other words, the CCFs can differentiate and extract the positive and negative sequences of each selected harmonic individually. (21) and (22) express a typical first-order CCF selected for the positive and negative sequences respectively of the aimed frequency.

$$G_{cff}{}^{p}(s) = \frac{w_p}{s - jh\widehat{w} + w_p} \tag{21}$$

$$G_{cff}{}^{n}(s) = \frac{w_p}{s + jh\widehat{w} + w_p} \tag{22}$$

Where w_p is the cutoff frequency.

Fig. 5 depicts the Bode magnitude diagram of a typical first-order CCF using (21), and a typical second-order BPF, where w_p is set to $2\pi 50$ rad/sec and ξ is set to 0.707. It is clear that the CCF offers a unit gain at the selected sequence, with a zero phase shift. On the other hand, the CCF offers an attenuated tuning to the nearby frequencies, whereas the second-order BPF offers a unity gain at both frequencies ($\pm w$) which implies that both polarities will pass the BPF with the same value. The MCCF-PLL proposed by [24] is depicted in Fig. 6. (a) Where each submodule is adjusted for a separated sequential component, and all the filtered sequential components are fed back to the input voltage as a mutual mode. The filtered positive sequence fundamental voltage is sent to the SRF-PLL to extract its phase, and the estimated frequency is fed back to the submodules to adapt the CCFs cutoff frequency during grid frequency variation. The basic structure of each submodule is illustrated in Fig. 6 (b) where k is set to 1 in case of extracting $v^{p}_{\alpha\beta h}$ and set to -1 in case of extracting $v^{n}_{\alpha\beta h}$. The mathematical formulations of the $v^{p}_{\alpha\beta 1}$ extracted by the CCFs are derived from Fig. 6. (b) as shown

$$v^{p}_{\alpha\beta 1} = \frac{w_p}{s - j\widehat{w} + w_p} \times \left(v_{\alpha\beta} - \sum_{h=1}^{m} \left[v^{p}_{\alpha\beta h} + v^{n}_{\alpha\beta h} \right] + v^{p}_{\alpha\beta 1} \right) \tag{23}$$

$$v^{p}_{\alpha\beta 1} = \frac{w_p}{s + w_p} \times \left(v_{\alpha\beta} - \sum_{h=2}^{m} v^{p}_{\alpha\beta h} - \sum_{h=1}^{m} v^{p}_{\alpha\beta h} + v^{p}_{\alpha\beta 1} \right) - \frac{\widehat{w}}{s + w_p} \times v^{p}_{\beta\alpha 1} \tag{24}$$

The design of the PI parameters of the MCCF-PLL is based on the transfer function expressed in (25), this latter is drawn from the open loop of the SRF-PLL that is depicted in Fig. 1. (a) [24].

$$G_{MCCF} = \frac{2\xi w_0 s + w_0^2}{s^2 + 2\xi w_0 s + w_0^2} \tag{25}$$

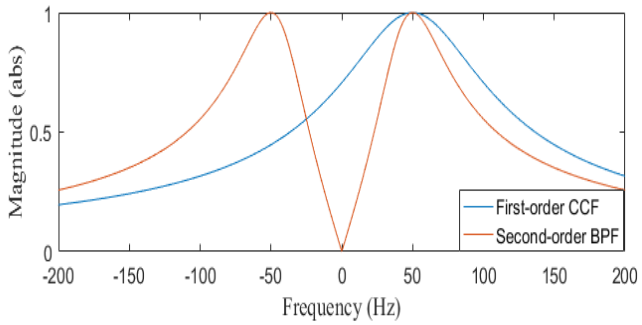

Fig. 5. Bode plot of first-order CCF and second-order BPF. Parameters:

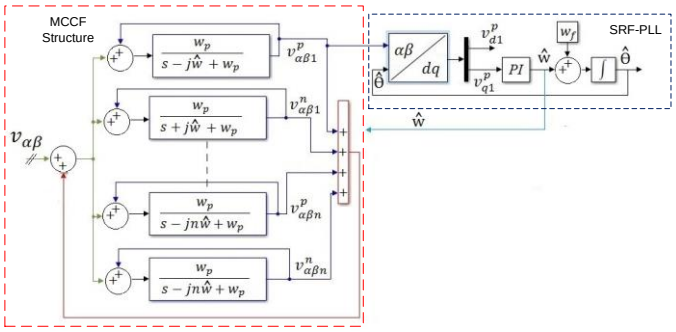

(a)

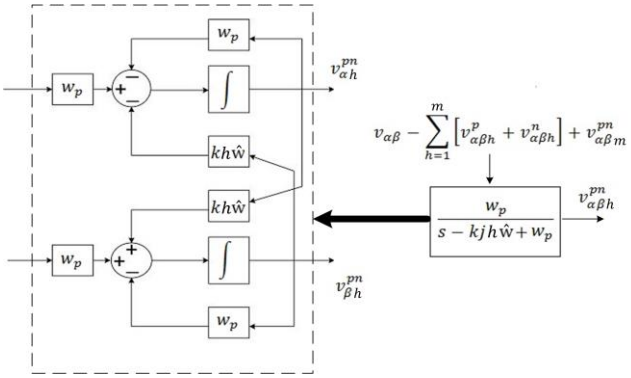

(b)

Fig. 6. Block diagram of MCCF-PLL. (a) Basic configuration. (b) Submodules configuration

Where ξ is the damping factor and in most cases it is selected as $\xi = k_p/(2\sqrt{k_i}) = 0.707$ for providing an optimal dynamic response. w_0 is set as $w_0 = \sqrt{k_i}$, where k_i can be adjusted to optimize the tradeoff between the high accuracy and the small transient response.

The MCCF-PLL, however, suffers from some weaknesses mainly the speed of the transient response before the filtering stage which depends on the phase of v_β as explained in section II. 1. Moreover, the tradeoff between improving the accuracy and reducing the transient response is still a challenge for the CCFs. Besides, the selective-property of the MCFF-PLL requires a large number of the filters in case the voltage is highly distorted which yields to increase the computation burden.

3. NLS approach overview

Contrary to the above-mentioned PLLs that are based on the closed-loop technique and require a careful design of the PI controller, the NLS approach is an open-loop technique that is unconditionally stable, and does not require any constraints of the controllers. The LS solution has been widely applied in several areas for harmonic extractions and frequency estimation and extended to APFs [26]-[29]. According to [26], the LS becomes nonlinear if the frequency of the grid is unknown or fluctuated in certain limit. The NLS approach can be expressed based on Fourier approximation [26]-[28], or based on Prony method (PM) [30], [31].

Suppose that $v_s(t)$ is the distorted voltage, according to PM method, $v(t)$ can be approximated by a sum of exponentials and residues as expressed in (26) [32].

$$v(t) \approx \sum_{i=1}^{\mathcal{p}} \Re_i \cdot e^{(\Im_i t)} + \aleph(t) \tag{26}$$

Where $v(t)$ is the observed voltage.

$\Re_i$ Residues of i poles.

$\aleph(t)$ Noise related to the measurement.

$\Im_i = -\theta_i + j\omega_i$.

θ_i damping factors of Poles.

ω_i Angular frequencies ($\omega_i = 2\pi f_i$).

In real applications, the filtering process is attained in the discrete time introducing a finite number of data samples Υ, and a sampling time T_s. Therefore, equation (26) can be expressed as

$$v(\ell T_s) \approx \sum_{i=1}^{\mathcal{p}} \Re_i \cdot \mathcal{g}_i{}^{\ell} + \aleph(\ell T_s) \tag{27}$$

Where: $\mathcal{g}_i = e^{(\Im_i T s)}$, the pole $\ell = 0,1, \ldots, \Upsilon - 1$, for the tolerance $\mathcal{p}$ we have $i = 1,2,\ldots\ldots \mathcal{p}$.

The purpose of this hypothesis is to find the best approximation of (27), based on NLS approach, this can be solved as

$$\underbrace{\begin{bmatrix} v(0) \\ v(1) \\ \vdots \\ v(\Upsilon-1) \end{bmatrix}}_{V} \approx \underbrace{\begin{bmatrix} 1 & 1 & \cdots & 1 \\ \mathcal{g}_1 & \mathcal{g}_2 & \cdots & \mathcal{g}_M \\ \vdots & \vdots & \ddots & \vdots \\ \mathcal{g}_1^{(\Upsilon-1)} & \mathcal{g}_2^{(\Upsilon-1)} & \cdots & \mathcal{g}_M^{(\Upsilon-1)} \end{bmatrix}}_{g} \underbrace{\begin{bmatrix} \Re_1 \\ \Re_2 \\ \vdots \\ \Re_M \end{bmatrix}}_{\Re} \tag{28}$$

$$\Re \approx g \backslash V \approx (g^T g)^{-1} g^T V \tag{29}$$

where V is the vector that contains the contaminated data, g is the introduced matrix that that contains the data of the aimed harmonics and $\Re$ is the extracted vector.

Based on the NLS method, inserting the data of g as a sinusoidal signal with a frequency of 50 Hz results in extracting the fundamental vector ($\Re$) of V. The amplitude of g is not important when extracting each frequency individually since the multiplication of $(g^T g)^{-1} g^T$ always leads to the same fixed amplitude. Although the NLS approach provides more accuracy comparing with the previous methods based on real and complex filters, it is a computational intensive technique that requires much care when implementing it on signal processor. However, since the aim of the algorithm is to extract only the fundamental signal of V, the multiplication $(g^T g)^{-1} g^T$ can be pre-computed offline, and the obtained data is run online and multiplied with V to give information about the fundamental component for each sampled point, which results in reducing the computation burden. Moreover, using the NLS approach to extract only the fundamental leads to reduce the matrix g to only one vector and thus decreases the calculation. Applying the NLS approach based on equations (27)-(29) uses only one vector, and offers an accurate extraction of the fundamental component. This latter is sampled in a moving window with a size of one cycle. Whereas the phase of the extracted fundamental is estimated using (30) and (31) in MATLAB. (30) Estimates the rank (Ra) and the magnitude (Ma) of the maximum point of the extracted buffered signal. For any sinusoidal signal, each cycle contains only one maximum point. Therefore, estimating Ra and multiplying it with the sampling time T_s as shown in (31), produces the phase of that signal but starting from the maximum point. Since the maximum point of a fundamental signal is shifted from the starting point by a quarter cycle ($\frac{\pi}{2}$), subtracting the obtained phase from $\frac{1}{f \cdot 4}$ that is corresponding to a quarter cycle (0.005s), offers accurate information of the phase ϕ of the start point of the signal.

$$[Ma\ Ra] = max\big(\Re(:)\big) \tag{30}$$

$$\phi = \left(Ra \cdot T_s - \frac{1}{f \cdot 4}\right) \cdot \frac{180}{0.01} \tag{31}$$

This technique of estimating ϕ reduces the computation burden, and provides information of ϕ for each sampled point in a moving window of one cycle.

The NLS approach, however, requires more computation compared to the above mentioned PLLs based techniques if it is applied to both voltage and current. Moreover, in case the dc offset appears, it requires one cycle to estimate the fundamental. Furthermore, the PF and the unbalance need extra calculation.

III. PROPOSED TECHNIQUES

In [26]-[28], the NLS approach is applied to the SAPF, but they did not consider the appearance odd harmonics and the dc offset in the voltage. Probably all the above mentioned filtering techniques require one or more than one cycle in case the voltage is contaminated with the odd harmonics and the dc offset.

Fig.7 depicts the proposed harmonic control methodology which is based on NLS approach. The strategy starts by transforming the voltage $V_{s1,2,3}$ from *abc* stationary frame to $\alpha\beta$ frame using (4). Then, $v_{\alpha,\beta}$ passes through a derivative, the role of this latter is to cancel the dc-offset of $v_{\alpha,\beta}$ in case it appears. Fig. 8 is added to clarify the steps of filtering v_α that is contaminated with harmonic components and dc offset of +50 V. Equation (32) illustrates the mathematical derivation of v_α. v_β is not depicted since it passes through the same procedures.

$$\frac{d\,v_\alpha}{dt} = \frac{d\,(v\sin(2\pi ft + \phi_h) + \sum_{h=2}^{m} v_h \sin(2\pi fht + \phi_h))}{dt}$$

$$= v2\pi f\sin(2\pi ft + \phi_h - 90^o) \sum_{h'=1,3,5..}^{m} v_h 2\pi fh' \sin(2\pi fh't + \phi_{h'} - 90^o)) \qquad (32)$$

where v is the amplitude of v_α.

According to (32), it is clear that when deriving v_α, the fundamental and all harmonics are multiplied respectively by $2\pi f$ and $2\pi fh'$, and shifted by -90^o. On the other hand, the dc offset is canceled. Since the objective is to extract the fundamental component, the derived signal $v_{\alpha d}$ is divided by a gain of $2\pi f$ to maintain the amplitude of the fundamental fixed when passing through the derivative as shown in Fig. 7 and 8. $v_{\alpha df}$ is extracted by applying the NLS approach. Equation (30) and (31) can extract the phase ϕ of $v_{\alpha df}$ when the moving window of the sampled data is set to one cycle (0.02s). However, when extracting $v_{\alpha df}$ using a moving window of a half cycle, obtaining Ra cannot be achieved if the buffered half cycle does not contain the maximum point. The reason is that, when separating a fundamental signal into two half cycles, one will contain information about the maximum point and thus Ra can be obtained, but the second one gives information about the minimum that cannot make an estimation of Ra. This impediment can be solved by estimating the absolute value of $v_{\alpha df}$ as shown in Fig. 7. Since the derivative guarantees the cancelation of the dc offset, the maximum and the minimum points of $v_{\alpha df}$ are equal in amplitudes. Therefore, applying the absolute function to $v_{\alpha df}$ ($|v_{\alpha df}|$) offers two similar positive half cycles, which implies that both of them contain the same Ra. As a result, the estimation of ϕ is accurately achieved using (33) and (34). For each buffered half cycle of $v_{\alpha df}$, if the absolute maximum point of $|v_{\alpha df}(:)|$ (max($|v_{\alpha df}(:)|$)) is bigger than the absolute minimum (min$(|v_{\alpha df}(:)|)$), this implies that the maximum point is located inside the buffered half cycle, and thus the algorithm estimates ϕ accurately. If max($|v_{\alpha df}(:)|$ is smaller than min$(|v_{\alpha df}(:)|)$, this means that the maximum point is not located in the buffered half cycle, and thus the algorithm adds a minus sign (-) to the estimated phase to indicate that the estimated phase is shifted by π. As a result, the estimation of ϕ for both half cycles is equal and accurate.

$$[Ma\ Ra] = max(|v_{\alpha df}(:)|) \qquad (33)$$

$$If \max(|v_{\alpha df}(:)|) > \min(|v_{\alpha df}(:)|) \Rightarrow \phi = \left(Ra \cdot T_s - \frac{1}{f \cdot 4}\right) \cdot \frac{180}{0.01}$$

$$else \;\; \phi = \left(Ra \cdot T_s - \frac{1}{f \cdot 4}\right) \cdot \frac{180}{0.01} \tag{34}$$

Once ϕ is obtained, it is subtracted from 90^0 to cancel the shift caused by the derivative, then, the sinusoidal fundamental signal is built again. Since v_α is shifted by $\frac{\pi}{2}$ from v_β, they are both generated to perform the SRF approach of the current $i_{l1,2,3}$ applying Park transform. The moving average filter is used to separate between the dc components (i_{ddc}, i_{qdc}) and the ripples (i_{dac}, i_{qac}) of the direct and inverse currents (i_d, i_q). The generated RCC are compared with the inverter output filter currents and the error is sent to the PWM control through a traditional PI controller, the gains of this latter are set to K_p =10.4 and K_i =0.1.

The application of NLS approach in $\alpha\beta$ frame reduces the number of filters and thus decreases the computation burden. The incorporation of the derivative cancels the dc offset, but it increases the noise as demonstrated in (32). In Fig. 8 the active filter is connected in the instant 0.03s, the high switching ripples of the inverter affects the voltage slightly. This affection is increased significantly when using the derivative and appears clearly on $v_{\alpha d}$. Using real and complex filters requires an expanded band to cancel the noise which is achieved on the cost of the response speed. However, it is clear in Fig. 8 that the NLS approach gives accurate estimation of the fundamental $(v_{\alpha df})$ under a noisy signal in only half cycle. As a result, the dynamic response of the

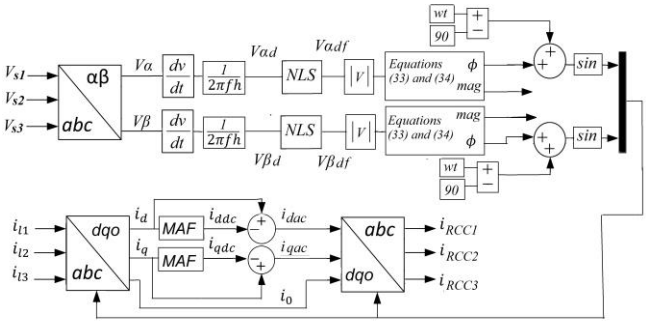

Fig. 7. the proposed methodology of harmonic control method.

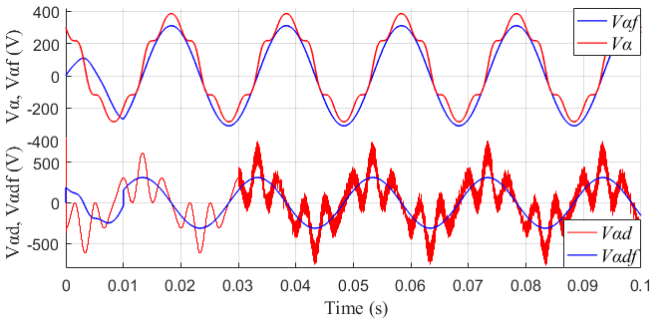

Fig. 8. the proposed methodology of harmonic control method

SAPF is improved and the computation burden of the algorithm is reduced.

IV. EXPERIMENTAL RESULTS

Fig. 9 depicts the shematic confuguration and the expiremental setup of the SAPF developed in the laboratory. The setup is consisted of a three phase programmable source (Chroma, model 61845), a three phase non-linear load. The algorithm is implimented under MATLAB blocks with a digital signal processor (dSPACE-1006). The SAPF is realized using Danfoss 2.2 kVA inverter with a switching frequency of 10 kHz and an output L-filter. The voltages and currents are sensed using Hall effect sensors. The sampling time is set to 0.0001 s. The dc-link capacitors are situated inside the setup. The parameters of the experimental system are summarized in Table I.

Fig. 10, 11 and 12 depict the practical results of the SAPF under distorted voltage (Fig. 10), distorted and unbalanced voltage (Fig. 11) and distorted voltage with dc offset (Fig. 12). The results are obtained using NLS approach based on the proposed strategy (Fig.10, 11 and12. (a)), the MCCF- PLL (Fig.10, 11 and12. (b)) and the MAF-PLL (Fig.10, 11 and12. (c)). According to Fig. 10. (a), (b) and (c), the voltage source $V_{s1,2,3}$ is contaminated by the harmonic components of the positive and negative

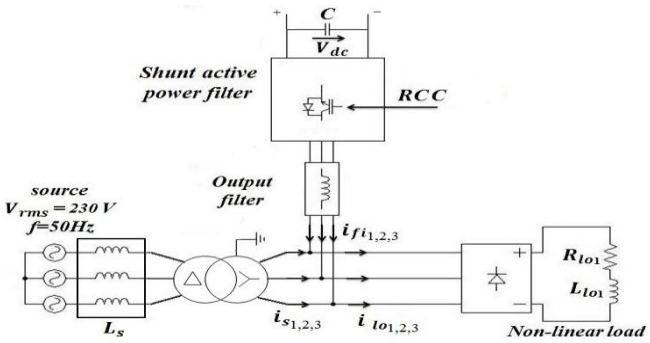

(a)

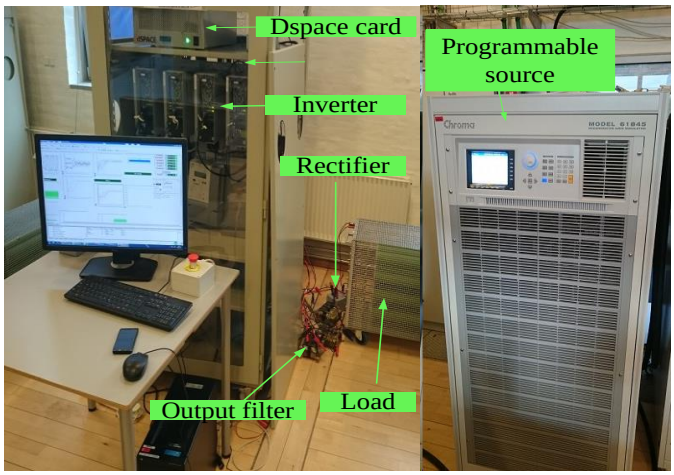

(b)

Fig. 9. Experimental prototype of the SAPF . (a) Schematic diagram of the SAPF. (b) Experimental setup of the SAPF.

sequences that are indicated in Table 1, with a total harmonic distortion (THD) of 15%. The filtered voltage $V_{sf1,2,3}$ is transformed back from $\alpha\beta$ stationary system to *abc* natural system to assess its response and accuracy. It is obvious that $V_{sf1,2,3}$ obtained by the proposed method takes only a half cycle to be filtered, whereas $V_{sf1,2,3}$ of the MCCF-PLL and MAF-PLL take more than one cycle to be stabilized and filtered. The load current $i_{lo1,2,3}$ is affected by the harmonic components of both voltage and non-linear load with a THD of 27%. The source current $i_{s1,2,3}$ of the three compared techniques are improved to reach a THD of less than 5% which respects the IEC 61000-3-6 and IEEE 519-1992 standards. However, $i_{s1,2,3}$ obtained by the proposed technique has the fastest transient response (0.0133s) that is clearly illustrated on the direct currents i_d and i_{ddc}. While $i_{s1,2,3}$ obtained by the other techniques take two cycles to reach steady state. i_{ddc} is filtered by a moving average filter, it is important to notice that since the dc offset and the odd harmonics do not exist, the band width of T_w is set to 0.02/6s to offer a faster transient response of i_{ddc}. The current $i_{fi1,2,3}$ is generated by the SAPF to the point of common coupling.

Table I. Practical parameters of the system

Power supply	Voltages RMS values:	
	Fundamental :	V_s = 230 V
	-5^{th} harmonic:	$V_{-5} = 30$ V
	7^{th} harmonic:	$V_7 = 20$ V
	-11^{th} harmonic:	$V_{-11} = 10$ V
	13^{th} harmonic:	$V_{13} = 5$V
	Main impedance:	$L_s = 0.005\ mH$
		$R_s = 0.5\ \Omega$
	Dc offset	$V_{s1,3} = +50$ V
		$V_{s2} = +100$ V
	Unbalance	$V_{s1,3} = 230$ V
		$V_{s2} = 180$ V
SAPF	dc link voltage references	$V_{dc} = 650$ V
	dc link capacitor:	C = 2200 μF
	output filters:	$L_f = 14\ mH$
		$R_f = 2.5\ \Omega$
Load	Non-linear load:	$R_L = 153\ \Omega$
		$L_L = 10$ mH

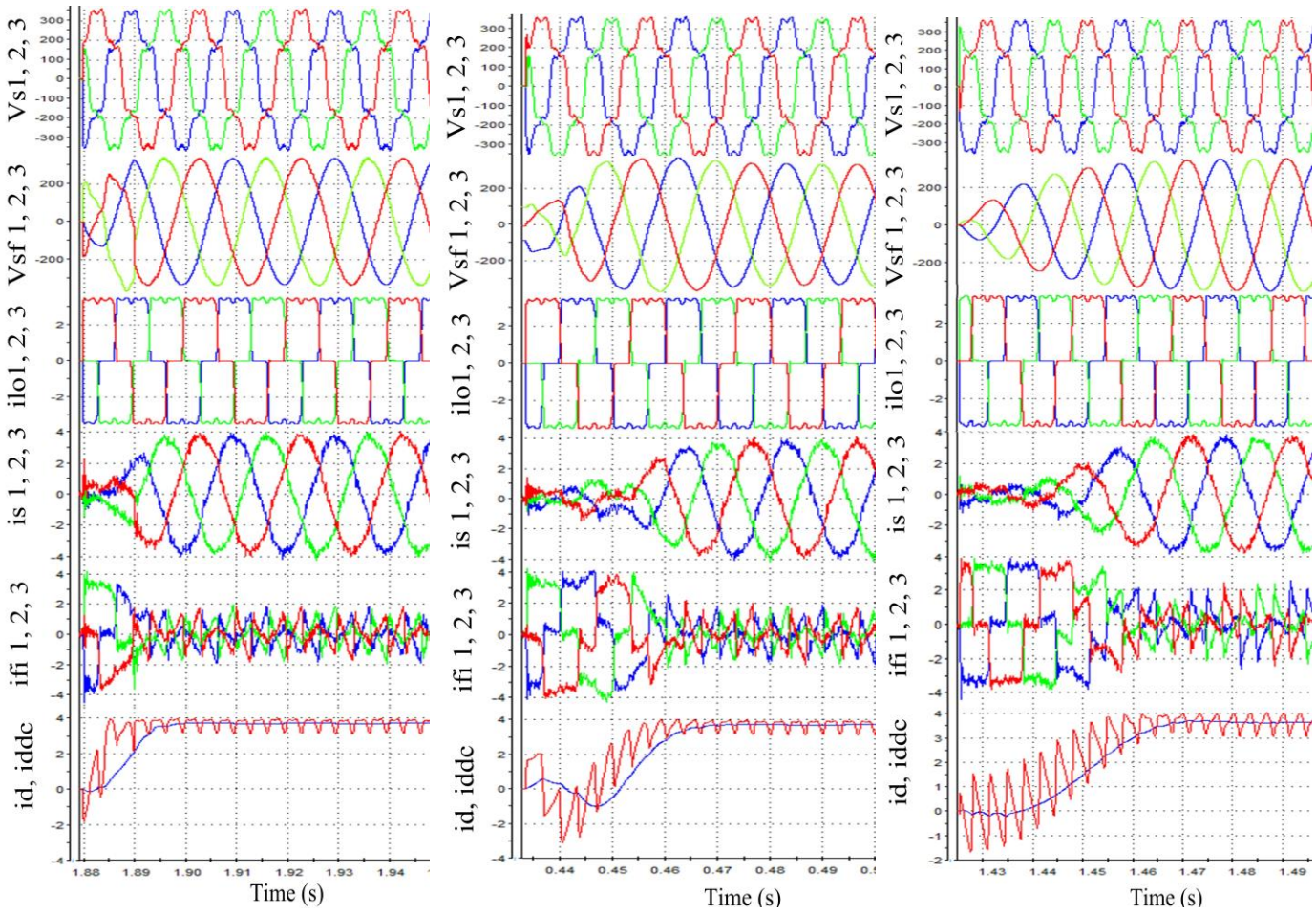

(a) (b) (c)

Fig. 10. Experimental results of SAPF in case of distorted voltage. (a) The proposed method. (b) MCCF-PLL. (c) MAF-PLL

According to Fig. 11. (a), (b) and (c), $V_{s1,2,3}$ is unbalanced and harmonically contaminated with the values that are indicated in Table 1. $i_{lo1,2,3}$ is affected by the harmonic components caused by the non-linear load and the unbalanced distorted voltage with different THDs (THD of $i_{lo1,3}$ is 25% and THD of i_{lo2} is 39%). It is obvious that even under the presence of harmonic components and unbalance, $V_{sf1,2,3}$ attained by the proposed method takes only half cycle to be filtered. While $V_{sf1,2,3}$ extracted by the other techniques takes approximately two cycles to be stabilized and filtered. As a consequence, $i_{s1,2,3}$ synchronized by the proposed technique takes only 0.15s to reach steady state with a THD less than 5%. Whereas $i_{s1,2,3}$ synchronized by the MCCF-PLL and MAF-PLL take respectively two cycles and more than two cycles to reach to steady state, which is noticeable on i_d and i_{ddc}.

In Fig. 12. (a), (b) and (c), $V_{s1,2,3}$ is contaminated with the harmonic components and dc offset, where the dc offset of phases 1 and 3 is set to 50V, while the dc offset added to the second phase is 100V, these values are selected exaggeratedly and higher than the dc offset that can happen in real application to demonstrate the effectiveness of the proposed technique under the worst cases. The fundamental of $V_{s1,2,3}$ is set to 200V. The wave form of $i_{lo1,2,3}$ is contaminated with different THDs (THD of $i_{lo1,3}$ is

28% and the one of i_{lo2} is 32%). Since the load is non-linear (three phase rectifier) and balanced, a three phase three wires inverter with one dc-link capacitor is sufficient to compensate for the harmonic contamination under adverse grid conditions. However, in case the non-linear load is unbalanced or linear with neutral, using another structure of the inverter such as three phase four wires inverter is mandatory. It is obvious that the appearance of dc offset does not affect the proposed technique in extracting $V_{sf1,2,3}$ within a half cycle. Whereas it causes slower time response to obtain $V_{sf1,2,3}$ (more than two cycles) using the MAF-PLL and MCCF-PLL. Moreover, it is clear that $V_{sf1,2,3}$ filtered by the CCFs still contain dc offset. The MCCF-PLL can be improved to cancel the dc offset, but that improvement is achieved on the cost of the response speed. In the case where the dc offset appear, the band width of the MAF applied to extract i_{ddc} is set to one cycle. As a result, $i_{s1,2,3}$ synchronized by the proposed technique takes 0.024s to reach steady state with a THD less than 5% which respects the abovementioned standards. However, the transient responses of $i_{s1,2,3}$ improved by the MAF-PLL and MCCF-PLL take roughly more than two cycles to reach steady state.

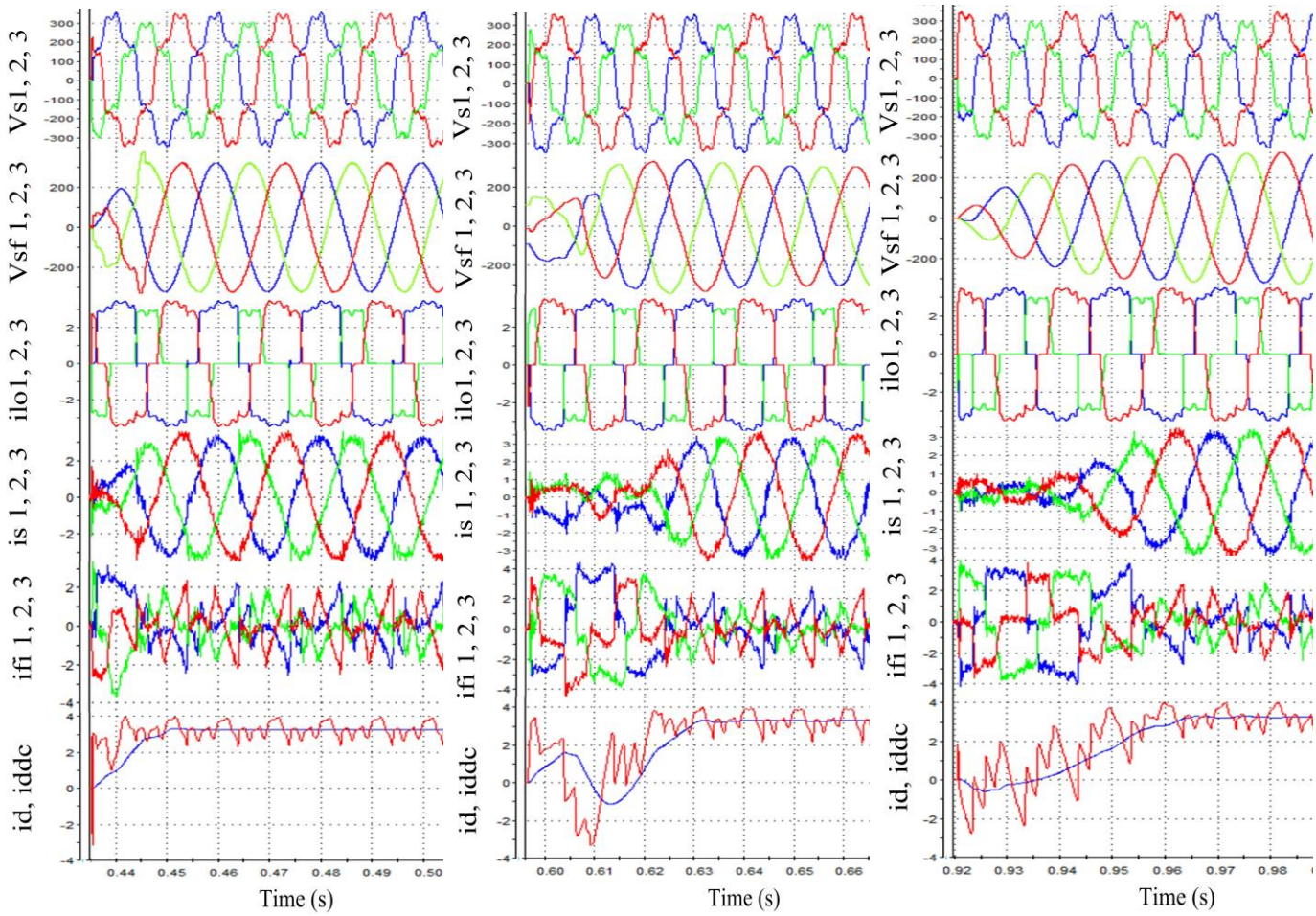

(a) (b) (c)

Fig. 11. Experimental results of SAPF in case of distorted unbalanced voltage. (a) The proposed method. (b) MCCF-PLL. (c) MAF-PLL

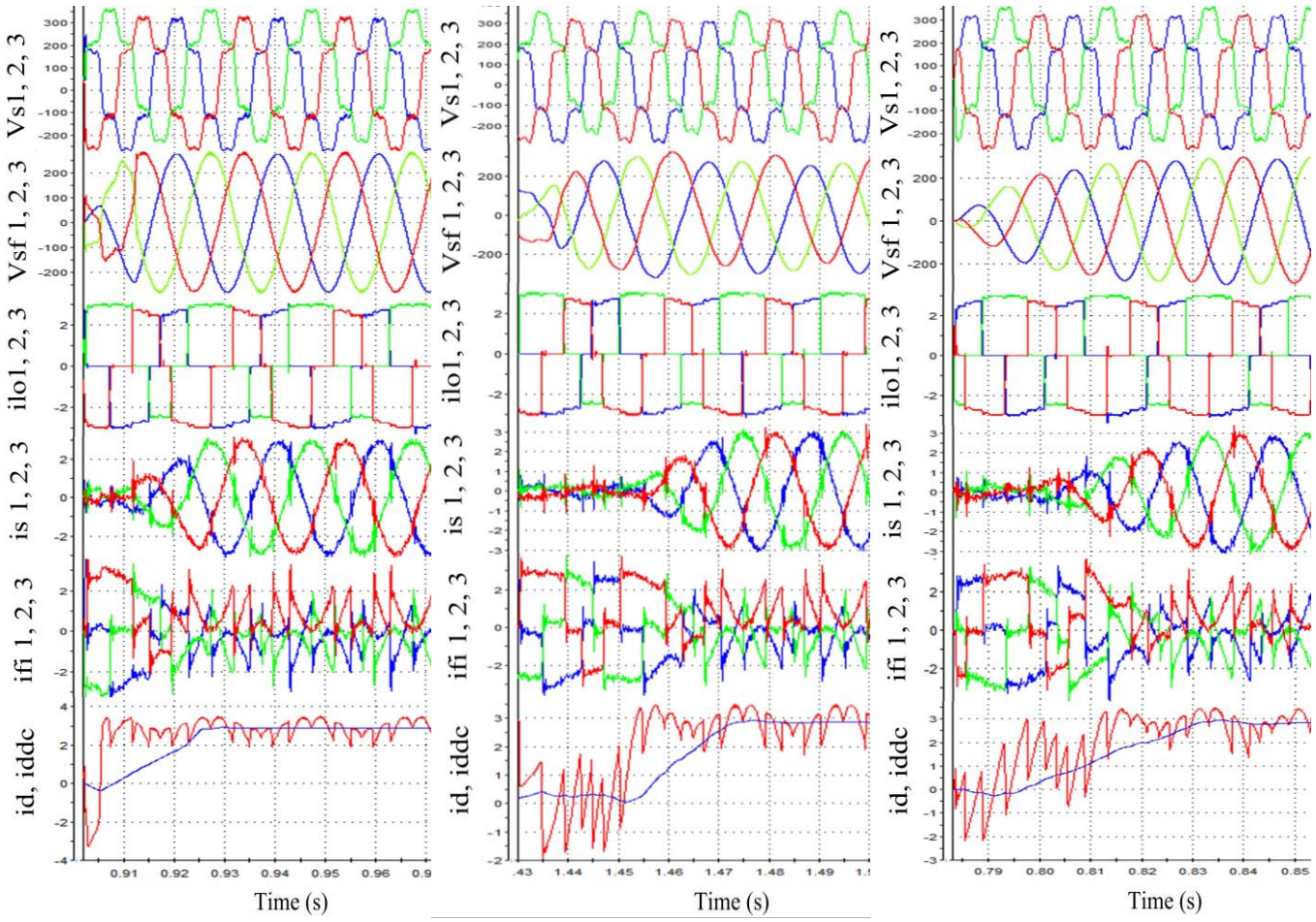

(a) (b) (c)

Fig. 12. Experimental results of SAPF in case of distorted unbalanced voltage. (a) The proposed method. (b) MCCF-PLL. (c) MAF-PLL

V. Conclusion

This paper proposes an improved open loop strategy based on NLS approach for synchronizing the RCC of the SAPF. The proposed techniques proved it is efficiency in extracting the fundamental component of the voltage and estimates its phase even under noise contaminated data. Moreover, the proposed method is compared with advanced PLLs (MCCF-PLL and MAF-PLL) to prove its accuracy and the fast dynamic response. The practical results showed that the advanced PLLs may require more than two cycles to synchronous the RCC of the SAPF. Whereas the proposed technique requires only a half cycle to provide an accurate estimation of the voltage phase in the presence of harmonic contamination, unbalance and dc offset. As a result, the dynamic response and the robustness of the SAPF are improved.

REFERENCES

[1] Smith, Robert L., and Ray P. Stratford. "Power system harmonics effects from adjustable-speed drives" *IEEE Trans. Ind. Appl*., vol. IA-20, no. 4, pp. 973-977, July 1984.

[2] J. S. Subjak and J. S. Mcquilink, "Harmonics—Causes, Effects, Measurements and analysis: An Update," *IEEE Trans. Ind. Appl*., vol. 26, no. 6, pp. 1-6,

Nov./Dec. 1990.

[3] R. Guzman, L. G. de Vicuña, J. Morales, M. Castilla and J. Miret, "Model-based control for a three-phase shunt active power filter," *IEEE Trans. Ind. Electron.*,vol. 63, no. 7, pp. 3998-4007, July 2016.

[4] K. Borisov and H. Ginn, "A novel reference signal generator for active power filters based on Recursive DFT," 2008 Twenty-Third Annual IEEE Applied Power Electronics Conference and Exposition, Austin, TX, 2008, pp. 1920-1925.

[5] C. V. Nunez-Noriega and G. G. Karady, "Five step-low frequency switching active power filter for network harmonic compensation in substations," *IEEE Trans. Power Del.*, vol. 14, no. 4, pp. 1298-1303, Oct 1999.

[6] Y.H. Juan, H.Y Huang, S.C Lai3, W.H Juang, "A distortion cancellation technique with the recursive DFT method for successive approximation analog-to-digital converters," *IEEE Trans. Circuits Syst. II, Exp. Briefs*, vol 63, no 2,pp. 146 – 150, 14 Aug 2015.

[7] A. Ovalle, G.Ramos, S. Bacha, A. Hably,and A.Rumeau," Decentralized control of voltage source converters in microgrids based on the application of instantaneous power theory," *IEEE Trans. Ind. Elec*, vol. 62, no.2, pp. 1152 – 1162, July 2014.

[8] A. Pigazo, V. M. Moreno and E. J. EstÉbanez, "A recursive park transformation to improve the performance of synchronous reference frame controllers in shunt active power filters," *IEEE Trans. Power Electron.*, vol. 24, no. 9, pp. 2065-2075, Sept. 2009.

[9] S. Golestan, M. Monfared and F. D. Freijedo, "Design-oriented study of advanced synchronous reference frame phase-locked loops," *IEEE Trans. Power Electron.*, vol. 28, no. 2, pp. 765-778, Feb. 2013.

[10] R. Cardoso, R. F. Camargo, H. Pinheiro, and H. A. Grundling, "Kalman filter based synchronisation methods," IET Gen., Transmiss., Distrib., vol. 2, no. 4, pp. 542–555, Jul. 2008.

[11] O. Vainio, S. J. Ovaska, and M. Polla, "Adaptive filtering using multiplicative general parameters for zero-crossing detection," *IEEE Tran. Ind. Electron.*, vol. 50, no. 6, pp. 1340–1342, Dec. 2003.

[12] P. Rodriguez, A. Luna, I. Candela, R. Mujal, R. Teodorescu, and F. Blaabjerg, "Multiresonant frequency-locked loop for grid synchronization of power converters under distorted grid conditions," *IEEE Trans. Ind. Electron*., vol. 58, no. 1, pp. 127–138, Jan. 2011.

[13] F. Bai, X. Wang, Y. Liu, X. Liu, Y. Xiang and Y. Liu, "Measurement-based frequency dynamic response estimation using geometric template matching and recurrent artificial neural network," in CSEE Journal of Power and Energy Systems, vol. 2, no. 3, pp. 10-18, Sept. 2016.

[14] Wenjie Zhang, Yicheng Liu, Xueguang Zhang and Dianguo Xu, "A novel grid voltage synchronization algorithm based on least mean square," Proceedings of The 7th International Power Electronics and Motion Control Conference, Harbin, China, 2012, pp. 2187-2192.

[15] S. Golestan, J. M. Guerrero and J. C. Vasquez, "Three-phase PLLs: a review of recent advances," *IEEE Trans. Power Electron.*, vol. 32, no. 3, pp. 1894-1907, March 2017.

[16] J. Wang, J. Liang, F. Gao, L. Zhang and Z. Wang, "A method to improve the dynamic performance of moving average filter-based PLL," *IEEE Trans. Power Electron.*, vol. 30, no. 10, pp. 5978-5990, Oct. 2015.

[17] S. Golestan, J. M. Guerrero, A. Vidal, A. G. Yepes and J. Doval-Gandoy, "PLL with MAF-based prefiltering stage: small-signal modeling and performance enhancement," *IEEE Trans. Power Electron.*, vol. 31, no. 6, pp. 4013-4019, June 2016.

[18] S. Golestan, M. Ramezani, J. M. Guerrero, F. D. Freijedo, and M. Monfared, "Moving average filter based phase-locked loops: Performance analysis and design guidelines," *IEEE Trans. Power Electron.*., vol. 29, no. 6, p. 2750–2763, Jun. 2014.

[19] E. Robles, S. Ceballos, J. Pou, J. L. Martin, J. Zaragoza, and P. Ibanez, "Variable-frequency grid-sequence detector based on a quasi-ideal lowpass filter stage and a phase-locked loop," *IEEE Trans. Power Electron*., vol. 25, no. 10, pp. 2552–2563, Oct. 2010.

[20] Y. F. Wang and Y. W. Li, "Three-phase cascaded delayed signal cancellation PLL for fast selective harmonic detection," ," *IEEE Trans. Ind. Electron.*, vol. 60, no. 4, pp. 1452-1463, April 2013.

[21] P. Rodriguez, J. Pou, J. Bergas, J. I. Candela, R. P. Burgos, and D. Boroyevich, "Decoupled double synchronous reference frame PLL for power converters

control," *IEEE Trans. Power Electron.*, vol. 22, no. 2, pp. 584–592, Mar. 2007.

[22] M. Ciobotaru, R. Teodorescu, and F. Blaabjerg, "A new single-phase PLL structure based on second order generalized integrator," in Proc. 37th IEEE Power Electron. Spec. Conf., Jun. 2006, pp. 1–6.

[23] I. Carugati, S. Maestri, P. G. Donato, D. Carrica and M. Benedetti, "Variable sampling period filter PLL for distorted three-phase systems," *IEEE Trans. Power Electron.*, vol. 27, no. 1, pp. 321-330, Jan. 2012.

[24] X. Guo, W. Wu and Z. Chen, "Multiple-complex coefficient-filter-based phase-locked loop and synchronization technique for three-phase grid-interfaced converters in distributed utility networks," ," *IEEE Trans. Ind. Electron.*, vol. 58, no. 4, pp. 1194-1204, April 2011.

[25] S. Golestan, M. Monfared, F. D. Freijedo and J. M. Guerrero, "Performance Improvement of a Prefiltered Synchronous-Reference-Frame PLL by Using a PID-Type Loop Filter," ," *IEEE Trans. Ind. Electron.*, vol. 61, no. 7, pp. 3469-3479, July 2014.

[26] R. Chudamani, K. Vasudevan and C. S. Ramalingam, "Real-Time Estimation of Power System Frequency Using Nonlinear Least Squares," *IEEE Trans. Power Del*., vol. 24, no. 3, pp. 1021-1028, July 2009.

[27] M. Qasim, P. Kanjiya and V. Khadkikar, "Artificial-Neural-Network-Based Phase-Locking Scheme for Active Power Filters," *IEEE Trans. Ind. Electron.*, vol. 61, no. 8, pp. 3857-3866, Aug. 2014.

[28] R. Chudamani, K. Vasudevan and C. S. Ramalingam, "Non-linear least-squares-based harmonic estimation algorithm for a shunt active power filter," in IET Power Electronics, vol. 2, no. 2, pp. 134-146, March 2009.

[29] M. D. Kusljevic, J. J. Tomic and L. D. Jovanovic, "Frequency Estimation of Three-Phase Power System Using Weighted-Least-Square Algorithm and Adaptive FIR Filtering," *IEEE Trans. Instrum. Meas.*, vol. 59, no. 2, pp. 322-329, Feb. 2010.

[30] R. Prony, "Essai experimentalet analytique, etc.," Paris J. 1'Ecole Polteclzmque, 1, cahier 2, 2476, (1795).

[31] T. K. Sarkar and O. Pereira, "Using the matrix pencil method to estimate the parameters of a sum of complex exponentials," *IEEE Trans. Antennas Propag*., vol. 37, no. 1, pp. 48-55, Feb. 1995.

[32] Sheshyekani, Keyhan, et al. "A general noise-resilient technique based on the matrix pencil method for the assessment of harmonics and interharmonics in Power Systems." *IEEE Trans. Power Del*., vol. PP,no.99, pp.1-1.